Contents lists available at ScienceDirect

Flow Measurement and Instrumentation

journal homepage: http://ees.elsevier.com

Experimental investigation of a cavitating Venturi and its application to flow metering

David Bermejo *, Xavier Escaler, Rafael Ruíz

C/Suïssa, 32, 08338, Premià de Dalt, Barcelona, Spain

ARTICLE INFO

Keywords
Cavitating Venturi
Choked flow
Sheet cavitation
Discharge coefficient
Flow rate coefficient
Flow metering

ABSTRACT

An experimental investigation has been carried out to evaluate the performance of a cavitating Venturi flow. For that purpose, a closed loop circuit with a centrifugal pump and a transparent asymmetric converging-diverging test section has been built which allows to set the pressure level and the flow rate. The system is instrumented with several pressure sensors and temperature probes that are continuously monitored during the tests. The experiments have consisted in generating non-cavitating and cavitating flows inside the Venturi under controlled conditions. The obtained results, which have been characterized as a function of the Venturi's discharge coefficient, pressure ratio and pressure loss coefficient, are in good agreement with previous studies carried out with standard Venturi geometries, specially under non-cavitating flows. The Venturi's performance under cavitation flows has been found to be dependent on the Venturi's inlet pressure and similar to a chocked flow condition with constant volumetric flow rate. On the basis of these observations and the analogous behaviour with compressible gas nozzles, a new flow coefficient has been derived which remains constant at any cavitating regime. Thus, this coefficient permits to use a Venturi as a flow meter on cavitation conditions.

Nomenclature

A
Cross section area $[m^2]$

C
Discharge coefficient $C = \frac{\dot{m}\sqrt{1-\beta^4}}{A_t\sqrt{2\rho(T)\,\Delta P}}$ $[-]$

ΔP
Pressure loss along Venturi tube $\Delta P = P_{in} - P_{out}$ $[Pa]$

$\dot{m}$
Mass flow rate $[kg/s]$

P
Pressure $[Pa]$

Q
Volumetric flow rate $[m^3/s]$

Re
Reynolds number $Re = \frac{\rho(T)\, v_{in}\, \varphi_{in}}{\mu(T)}$ $[-]$

T
Thermodynamic temperature $[K]$

v
Area averaged velocity $v = \frac{Q}{A}$ $[m/s]$

Greek characters

β
Contraction ratio $\beta = \frac{\varphi_t}{\varphi_{in}}$ $[-]$

Θ
Flow rate coefficient $\Theta = \frac{Q}{A_t\sqrt{\frac{P_{in}}{\rho(T)}}}$ $[-]$

φ
Hydraulic diameter $[m]$

μ
Dynamic viscosity $[Pa\,s]$

ρ
Density of liquid phase $[kg/m^3]$

σ
Cavitation number $\sigma = \frac{P_{out} - P_{sat}(T)}{\frac{1}{2}\rho(T)\, v_t{}^2}$ $[-]$

ζ
Pressure loss coefficient $\zeta = \frac{P_{in} - P_{out}}{\frac{1}{2}\rho(T)\, v_t{}^2}$ $[-]$

Subscripts and superscripts

ref
Referred to idle conditions (i.e. stopped pump)

* Corresponding author.
E-mail address: david.bermejo@upc.edu (D. Bermejo)

https://doi.org/10.1016/j.flowmeasinst.2020.101868
Received 7 January 2020; Received in revised form 10 September 2020; Accepted 6 December 2020
Available online xxx
0955-5986/

sat
Referred to water's saturation state
in
Referred to Venturi's inlet section
out
Referred to Venturi's outlet section
t
Referred to Venturi's throat section

1. Introduction

Both liquid and gas states of matter coexist in equilibrium until a driving force appears causing an imbalance between both and a mass transfer takes place. Mass transfer from gas state to liquid one is known as condensation while the reverse phenomenon is called vaporization [1]. For the latter, the mass transfer is led by temperature gradient in boiling process –liquid is heated until saturation pressure reaches local pressure– but when the driving force which leads the mass transfer is a pressure gradient then cavitation takes place –local pressure drops until saturation temperature reaches local temperature–. In the present work we have focused on cavitation in flowing water.

It is well known that subsonic fluids flowing through converging-diverging geometries, such as Venturi tubes, suffer of an exchange between pressure and kinetic energy in order to accelerate or decelerate: in converging section the pressure decreases in favour of fluid's velocity but in diverging sections the exchange takes place reversely. Hence, the flow experiments its lowest pressure and highest velocity across the throat's section, which corresponds to the smallest cross-sectional area. Therefore, a liquid (incompressible fluid) flowing through a converging-diverging geometry might experiment the formation of vapour bubbles in the throat's section at a suitable flow rate due to cavitation exhibiting a compressible behaviour.

Converging-diverging geometries with circular cross section are commonly used for flow rate measurements in flowing gases [2] and liquids [3] when no cavitation occurs based on the pressure difference between inlet and outlet sections (ΔP). The geometry proposed for gases is a classical Venturi tube while the one proposed for liquids is a Herschel-Venturi –the throat is enlarged for a length equal to the throat's diameter φ_t–. In both cases, they have slight converging/diverging angles and long diverging sections. The experiments have demonstrated that they present a constant discharge coefficient and a low uncertainty inside a given range of operation without cavitation. The discharge coefficient, C, is defined by Ref. [3] with:

$$C = \frac{\dot{m}\sqrt{1-\beta^4}}{A_t\sqrt{2\rho(T)\,\Delta P}} \tag{1}$$

$$\beta = \frac{\varphi_t}{\varphi_{in}} \tag{2}$$

where the measurement of ΔP is used to calculate the mass flow rate, $\dot{m}$, through the pipe. Typical range of values for C are from 0.957 to 0.995 as indicated by Ref. [3].

Under cavitation conditions, Venturi tubes are choked and present an exceptional behaviour for flow control but they have not been used for flow metering yet because under such conditions the discharge coefficient is no longer constant. Due to the fact that the flow rate is chocked, i. e. constant, in choked regime, cavitating Venturi flow is used in industries where flow control is critical such as in liquid propellant rockets as presented in the works of Randall [4] and Ulas [5].

Several studies have employed a Venturi type geometry with circular cross section to generate cavitation thanks to its excellent balance between construction simplicity, low cost and flow conditions reproducibility. For example, Zamoum et al. [6], Abdulaziz [7] and Rudolf et al. [8] carried out experiments to study the cavitation morphology and cavitating Venturi's performance through the measurement and analysis of flow rates and pressure losses. Others like Charrière et al. [9] and Brinkhorst et al. [10] conducted numerical simulations to validate cavitation models. Other studies, like those presented by Dular et al. [11] and Decaix et al. [12], a Venturi with a rectangular cross section was used to study the cavitation structures and dynamic behaviour.

The cavitation phenomenon can be characterized with the non-dimensional cavitation number which is defined as the ratio between the outlet's pressure relative to the saturation pressure and the dynamic pressure measured in the throat's section:

$$\sigma = \frac{P_{out} - P_{sat}(T)}{\frac{1}{2}\rho(T)\,v_t^2} \tag{3}$$

where the saturation pressure, $\boldsymbol{P_{sat}(T)}$, is calculated as a function of the water temperature by means of the formulation proposed by the International Association for the Properties of Water and Steam [13].

The dimensionless pressure loss coefficient through a pipe or a component of an hydraulic circuit is defined by:

$$\zeta = \frac{P_{in} - P_{out}}{\frac{1}{2}\rho(T)\,v_t^2} \tag{4}$$

The pressure loss coefficient characterizes the resistance of hydraulic components such as elbows, valves or orifice plates. Moreover, it has also been used to study the performance of different Venturi geometries at different operational regimes comprising both non-cavitating and cavitating conditions [8,14].

As pointed above, converging-diverging geometries have not been used as flow metering devices under cavitation conditions yet. Instead, they are being employed as flow control devices because the flow rate remains invariable in front of downstream pressure fluctuations. Nevertheless, the discharge and the pressure loss coefficients –the most extended dimensionless numbers used for characterizing and comparing geometries– are no longer constant when cavitation appears. Thus, a new flow coefficient must be defined if Venturi geometries are expected to be used as flow meters under cavitating regimes.

This paper presents the experimental investigations carried out in a closed loop circuit to determine the effects of cavitation on the performance of a rectangular cross section Venturi and proposes a new flow coefficient for flow metering under cavitating regimes. Firstly, the test-rig allowing to control the flow rate and pressure levels and the observed cavitation regimes within the Venturi are described. Then, the experimental procedure and the set of experiments are described. The obtained results are presented and discussed with detail demonstrating a strong dependency between the flow rate and the Venturi's inlet pressure in cavitating regimes. As a result, a new flow coefficient is proposed and validated which overcomes most accepted coefficients. The proposed flow coefficient remains constant during cavitation conditions allowing to infer the flow rate for any operating range by means of a single static pressure measurement at the Venturi's inlet section.

2. Experimental device and set-up

2.1. Experimental set-up

The test-rig employed for the present experimental study is shown in Fig. 1. This cavitation tunnel is a closed loop circuit made in PVC pipes and powered by a 3 kW LOWARA SHE 40–160/30 centrifugal pump. One large reservoir –filled with 30 L of tap water– is located between the pump's discharge pipe and the Venturi's inlet section in order to damp the pressure and flow rate fluctuations. The presence of a free

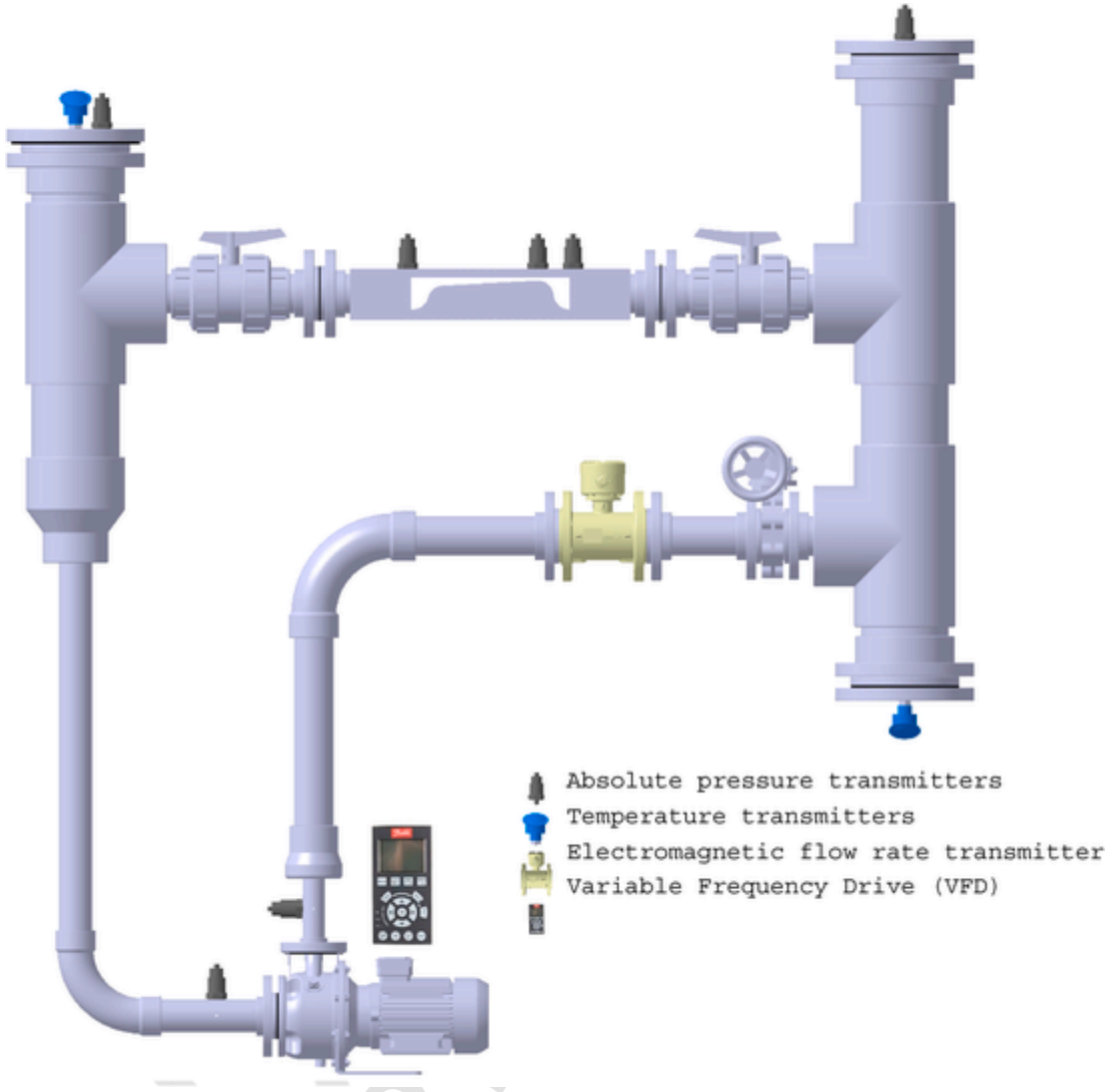

Fig. 1. Cavitation tunnel powered by a 3 kW centrifugal pump and controlled with a variable frequency drive (VFD) and a valve placed downstream the flowmeter.

surface combined with the isolation of the whole system with respect of the ambient pressure, contributes to damp eventual fluctuations (see Bermejo et al. [14] for more details).

The system's flow rate is set with the rotating speed of the pump and the opening ratio of the butterfly valve located downstream the flowmeter (see Fig. 1). The pump's rotating speed is controlled with a variable frequency drive (VFD). The maximum system's flow rate is about 41.5 m^3/h. The system's reference pressure (P_{ref}) is defined as the free surface pressure inside the suction reservoir in idle conditions and it is set by means of a pneumatic control system that permits to pressurize and make vacuum. The range of absolute pressures that can be achieved are from 10 kPa to 1.1 MPa. The water temperature, measured by means of two transmitters placed on both reservoirs, shifts freely during each experimental trial. However, initial conditions can be repeated by refilling the test-rig with fresh water. The 3D CAD model of the piping circuit was used to calculate the system's volume, which has 78 L, approximately.

The centrifugal pump is isolated from the rest of the components by means of two expansion joints placed upstream and downstream and it is attached to the frame through three silent blocks in order to reduce the transmission of vibrations from the pump to the test section. The AISI 304 frame that supports the main components is isolated from the floor with four silent block adjustable legs.

The system is instrumented with several sensors comprising seven (7) absolute pressure transmitters E&H Cerabar PMC-11 and two (2) temperature transmitters PT100 Class A WIKA TR11-C. Two absolute pressure transmitters are employed for measuring the pump's head which are mounted with ring manifold following the ISO 9906:2012 [15] recommendations. The rest of pressure transducers are located in both reservoirs and along the Venturi test section. The two temperature transmitters are located inside the two reservoirs. Moreover, an electromagnetic flowmeter ABB ProcessMaster300 FEP311 and a pump's VFD provide output signals for volumetric flow rate and the rotating speed measurements.

A graphical user interface was programmed in LabVIEW® for monitoring the operating conditions of the cavitation tunnel in real time. The data acquisition system reads the signals with a current module NI-9208.

2.2. Venturi

A Venturi with a total length of 375 mm between inlet and outlet sections and with rectangular cross sections was designed and used for the present study in contrast with other Venturi geometries studied in Refs. [7,10,16] which all were axisymmetric. Both inlet and outlet sec-

tions have a square cross section of 72 mm of side and smoothly progress to a circular cross section to be coupled to PVC pipes.

The lateral view of the Venturi and its main dimensions are outlined in Fig. 2. As can be seen, the Venturi has a flat upper wall with three orifices at the outlet, throat and inlet sections (from right to left) for flush mounted pressure transmitters. The static pressure taps for each pressure transmitter were designed following the ISO 9906:2012 guidelines [15] to prevent the influence of turbulence in the measures. The sensor at the throat section was selected with a pressure range from 0 to 2.0 MPa, and the two other sensors had a range from 0 to 6.0 MPa.

The Venturi's converging section presents a contraction ratio β of 0.173 from an inlet square section to a throat of 6.8 mm of height through soft edges. This geometry is similar to those tested in Ref. [7] but with the exception that it has an asymmetric diverging section with respect to the throat plane. The throat cross area is of 490 mm^2, it has 12.4 mm of hydraulic diameter and it is not elongated like the Herschel's geometries tested in Ref. [10]. Consequently, the maximum area average velocities are 2.22 m/s and 23.5 m/s at the Venturi inlet and throat sections, respectively. And the Reynolds number at the inlet section is 1.88×10^5. The diverging section extends from the throat for 216 mm with a diverging angle of 3°, which corresponds to the lower range of diverging angles recommended by ISO 9300 [2].

2.3. Cavitation regimes

The transparent Venturi walls made with PMMA (polymethyl methacrylate) permit the visualization of the cavitation phenomena through both lateral windows and from the upper wall.

During the set-up of the cavitation tunnel and in preliminary experiments presented in Ref. [14], four different flow regimes were identified attending to the length of the attached cavity, as shown in Fig. 3: non cavitating (a), partial cavitation (b), full cavitation (c) and supercavitation (d).

In partial cavitation, the attached sheet of cavitation ends within the diverging section of the Venturi, meanwhile for full cavitation the cavity closure occurs inside the outlet's pipe. And for supercavitation, the cavitation enters inside the suction reservoir.

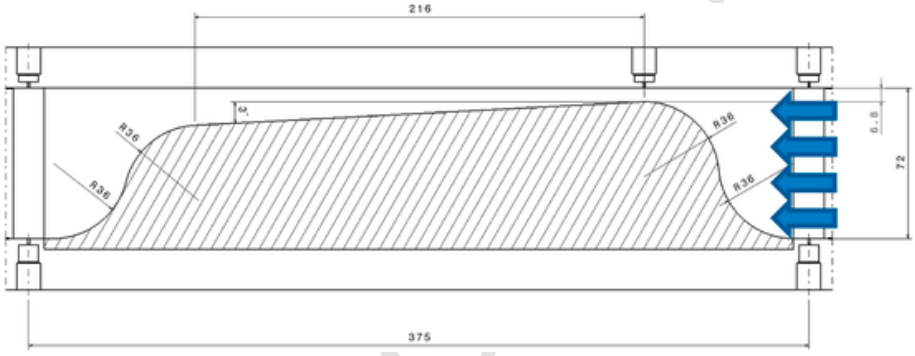

Fig. 2. Lateral view of the Venturi and main dimensions (flow from right to left). Pressure taps are located in inlet, throat and outlet sections on the upper wall. Two extra pressure taps were practice in inlets and outlet sections on the bottom wall as reserve.

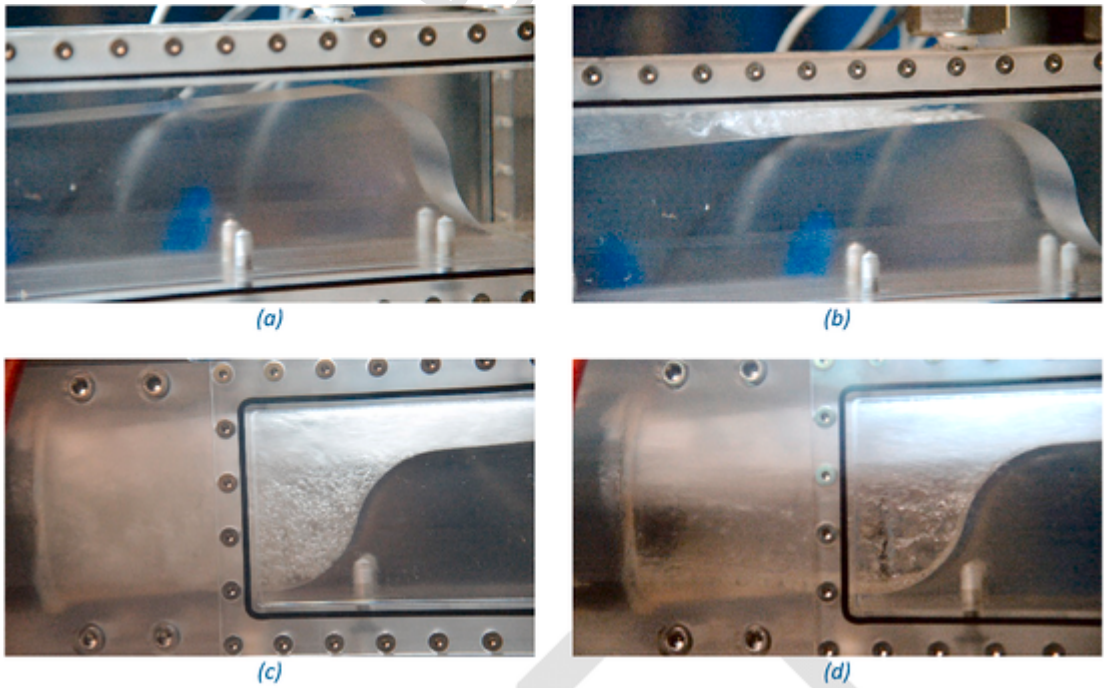

Fig. 3. Pictures of observed cavitation regimes in the Venturi with flow from right to left: non-cavitating (a), partial cavitation (b), full cavitation (c) and supercavitation (d). Images (a) and (b) show Venturi's inlet section and images (c) and (d) show the Venturi's outlet section.

3. Experimental procedure

3.1. Degassing process

The presence of dissolved gasses in the bulk water affects the behaviour of cavitation acting as nuclei. As reported by Brennen [1], the amount of nuclei reduces the required energy and increases the pressure at which cavitation appears. Degassing the system consists in promoting the mass transfer of dissolved gasses from liquid to gas phase by means of changing the equilibrium state with a reduction of the P_{ref} and displacing the equilibrium to a new state with a lower concentration of dissolved gas, i.e. with less cavitation nucleis. Therefore, the water had to be degassed at the beginning of each test or when it had been renewed.

The process of degassing consisted in running the system in close to vacuum conditions with absolute P_{ref} values between 10 and 12 kPa in full cavitation regime. As can be seen in Fig. 4, the pressure rises steadily at a different rates depending on the amount of nuclei while degassing takes place. Therefore, the pressure recovery rate during the test is used as an indicator of the presence of dissolved gas.

The plot in Fig. 4 shows that, at the beginning of the degassing process, the pressure recovery rate is higher due to the large amount of gasses dissolved inside the liquid. For example, the pressure increases around 50 kPa every 5 min at the beginning of the first run. But the pressure only increases 14 kPa every 5 min at the end of the same run. When several degassing runs have been carried out, the slope of the pressure recovery becomes constant and corresponds to the system's leak rate. For example, the last complete run presents a rate of about 0.6 kPa every 5 min when the starting pressure is 10 kPa. Below this point, even if we increase the pressure to 19 kPa and stop the flow, the pressure recovery rate is approximately the same with a value of 0.7 kPa every 5 min, which confirms that the amount of absorbed gas in the bulk liquid has been reduced to its minimum.

3.2. Tests carried out

The set of tested operating points was chosen based on the system's reference pressure and the volumetric flow rate. The measured temperature range was from 12 to 30 °C for all tests.

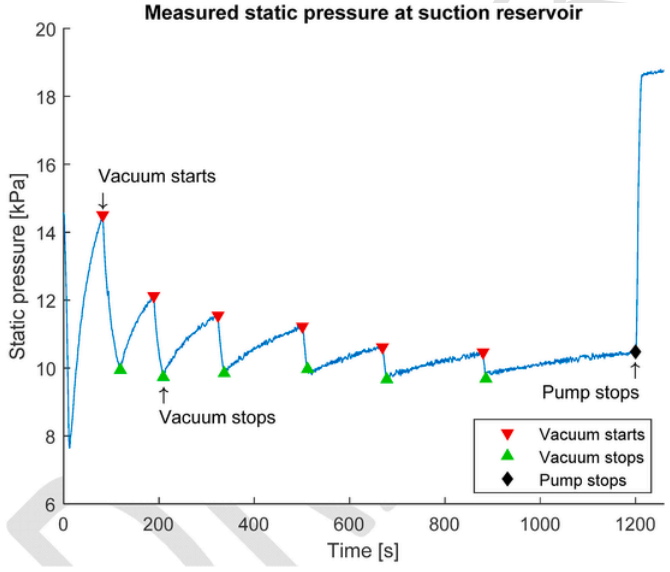

Fig. 4. Static absolute pressure measured in the suction tank during several degassing processes running at vacuum conditions with supercavitation. As the liquid is degassed, the pressure recovery slope decreases and tends to stabilize.

A series of repetitive tests were carried out for seven (7) levels of P_{ref} comprising 70, 90, 100, 110, 130, 150 and 200 kPa. For each P_{ref}, fourteen (14) opening ratios of the control valve from fully closed to fully opened and six (6) pump's rotating speeds from 50 to 100% of the nominal speed in steps of 10% were selected, resulting into a total of 1176 operational points.

Each session of tests has been started with a degassing process, followed by a system pressurization at zero speed for purging the pressure transducers. The reference pressure has been firstly set and then the control valve has been adjusted. For each control valve position, six (6) measurements of 60 s each one have been carried out from the lower rotating speed till the highest one. Before starting each measurement, the system has been left running for a prudential period of time in order to fade eventual transient fluctuations. When the temperature has reached 30 °C, the session has been stopped, the water has been renewed and the testing procedure has been restarted again from the degassing process.

3.3. Measurement of uncertainty

The uncertainties of the direct and derived measurements were carefully estimated following the guidelines of the Joint Committee for Guides in Metrology [17] and taking into account the stochastic uncertainty of the variables and those systematic uncertainties coming from the measurement hardware. Stochastic uncertainty was controlled by using a sampling rate of 5 Hz per channel and calculating the average and standard deviations every second. In order to control the systematic uncertainties of the system, the pressure, temperature and flowmeter transmitters were calibrated.

All the measurements were averaged during 60 s in steady operating conditions. Fig. 5 shows the stability of (a) the Venturi's inlet pressure, (b) Venturi's throat pressure, (c) flow rate and (d) cavitation number, respectively, during one trial. The highest relative uncertainty of the inlet pressure is ± 2 kPa at 249 kPa corresponding to a relative uncertainty below 1%. For the throat pressure measurement, the maximum uncertainty calculated is ± 1.7 kPa at 41.5 kPa, corresponding to a relative uncertainty below 4%. For the volumetric flow rate and the cavitation number the relative uncertainty is also below 1% with maximum values of ± 0.3 m^3/h at 40.5 m^3/h and ± 0.007, respectively.

4. Results

4.1. Flow rate vs Reynolds

To characterize the flow in the Venturi the Reynolds number was calculated based on the hydraulic diameter of the Venturi's inlet section and its averaged velocity which, in turn, was calculated using the averaged volumetric flow rate and its area. The influence of the temperature on the density and dynamic viscosity was also taken into account according to Refs. [13,18].

$$Re = \frac{\rho(T)\, v_{in}\, \varphi_{in}}{\mu(T)} \tag{5}$$

$$Re = \frac{\rho(T)}{\mu(T)} \frac{\varphi_{in}}{A_{in}} Q \tag{6}$$

The volumetric flow rate has been plotted as a function of the Reynolds number for the measurements in Fig. 6. As it can be seen, the represented operating points fall inside a cone formed by the lines corresponding to equation (6) particularized for 10 and 30 °C (see dotted straight lines in Fig. 6), demonstrating the dependency on the water temperature. An increase of the water temperature leads to an increase of the Reynolds number for a given flow rate. In addition, it can be confirmed that the flow was fully turbulent at the inlet section of the

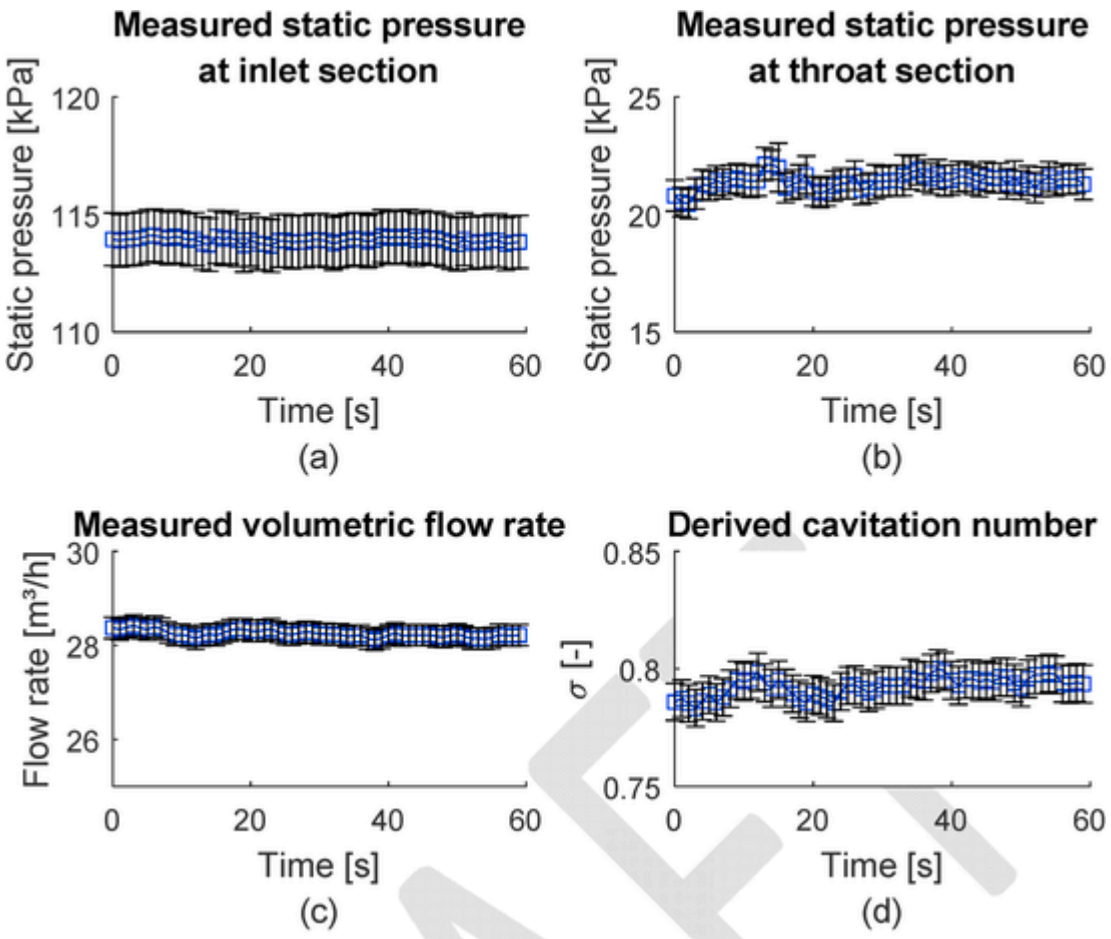

Fig. 5. Measured variables and associated uncertainty of (a) Venturi's inlet pressure, (b) Venturi's throat pressure, (c) volumetric flow rate and (d) calculated cavitation number.

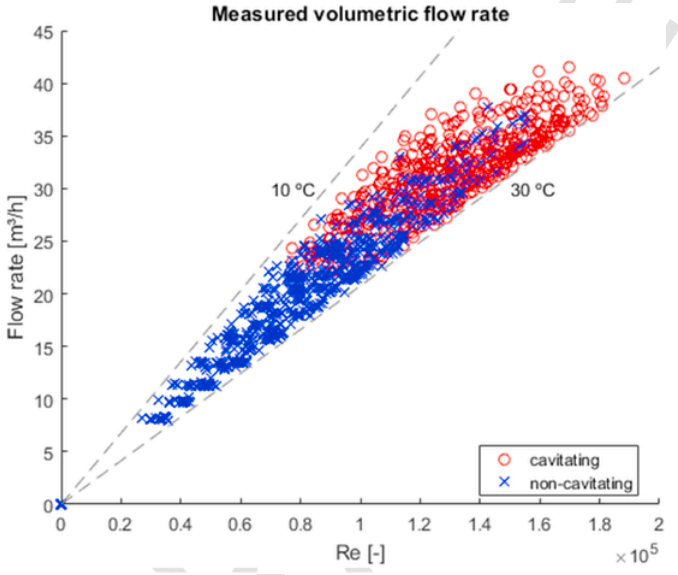

Fig. 6. Measured volumetric flow rate as a function of Reynolds number. The dashed lines represent theoretical values for water temperatures of 10 and 30 °C. Blue crosses correspond to non-cavitating regime and red circles correspond to cavitating regimes. (For interpretation of the references to colour in this figure legend, the reader is referred to the Web version of this article.)

Venturi since the Reynolds was within the range from 2.7×10^4 to 1.9×10^5, clearly above the accepted critical value of 3×10^3 [19].

4.2. Flow rate vs pressure ratio

The volumetric flow rate has been represented as a function of the pressure ratio between the Venturi's outlet and inlet section pressure values in Figs. 7 and 8. The resulting plot in Fig. 7 shows two different behaviours below or above a pressure ratio between 0.67 and 0.71. Above this threshold region, the flow rate decreases following a quadratic trend when the pressure ratio increases. These points exhibit different trends depending on P_{ref} and, for a constant pressure ratio, the flow rate increases with P_{ref}. Below that threshold, the flow rate remains constant for constant P_{ref} as the pressure ratio decreases. This change of behaviour is due to the presence of cavitation which was observed for pressure ratios below $0.67 \div 0.71$ meanwhile the upper region corresponds to operating regimes without cavitation. The cavitation inception was assessed by visual observation combined with audible sound during the experiments.

Authors like Abdulaziz [7] or Brinkhorst et al. [20] studied the flow rate through converging-diverging pipes for different downstream pressures while keeping constant the upstream pressure too. They found out that, at cavitating regimes, the mass flow was constant for any downstream pressure, confirming that the flow was choked and in accordance with our observations. Moreover, the threshold between both regimes takes place at a very similar pressure ratio located between 0.7 and 0.72 in the experiments of Abdulaziz [7] despite the difference be-

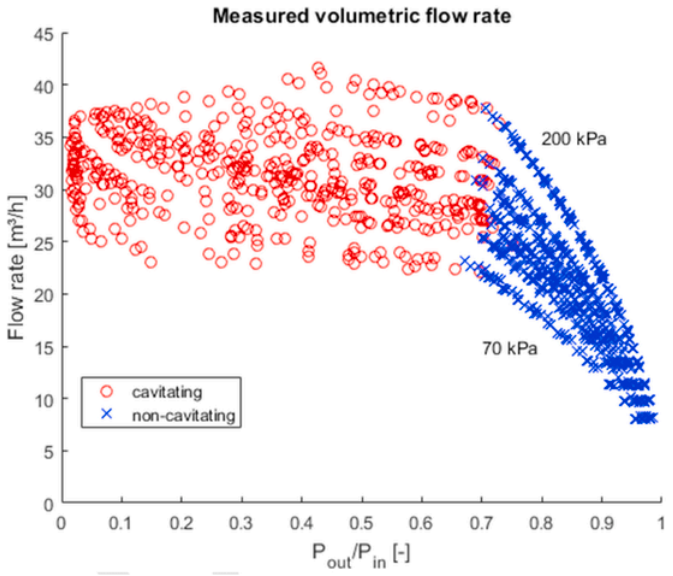

Fig. 7. Measured volumetric flow rate as a function of the pressure ratio between Venturi's outlet and inlet section. Blue crosses correspond to non-cavitating regime and red circles represent cavitating regimes. The cavitation inception was assessed by visual observation. (For interpretation of the references to colour in this figure legend, the reader is referred to the Web version of this article.)

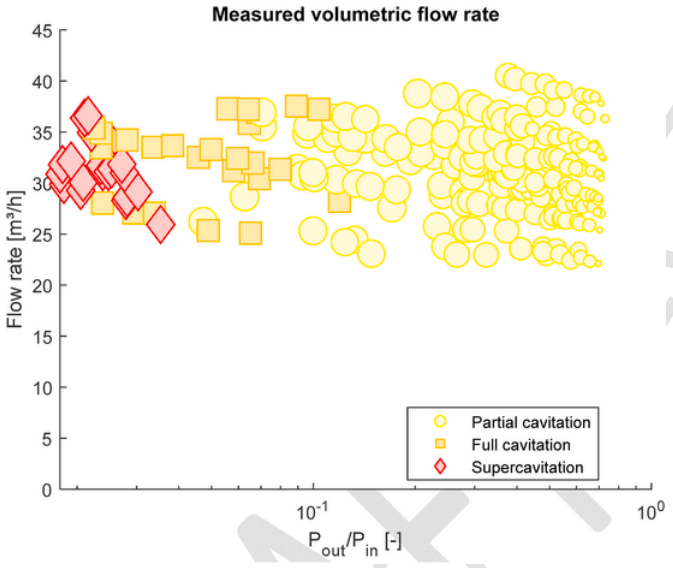

Fig. 8. All three cavitation regimes identified in Fig. 3 (partial cavitation, full cavitation and supercatitation) are presented as a function of measured volumetric flow rate and pressure rate. The size of the markers represents the length of the observed cavity.

tween their geometry (which was an axisymmetric Venturi with a converging/diverging angle of 6.2°) and our geometry.

The cavitation regimes described in Fig. 3 are grouped together in Fig. 8 where partial cavitation extends from pressure rates of 0.71 to 0.11 (represented by yellow circles). Orange squares represent full cavitation operating points, which extend from pressure rates of 0.12 to 0.02. The region bellow 0.04 corresponds to supercavitation (represented with red diamonds). The size of each marker is proportional to the corresponding cavity length.

4.3. Flow rate vs cavitation number

The volumetric flow rate has been represented as a function of the cavitation number in Fig. 9. The flow rate exhibits an inverse dependency to the square of cavitation number and a strong dependency with the reference pressure level P_{ref}. Abdulaziz [7] also detected this pressure dependency as a function of cavitation number.

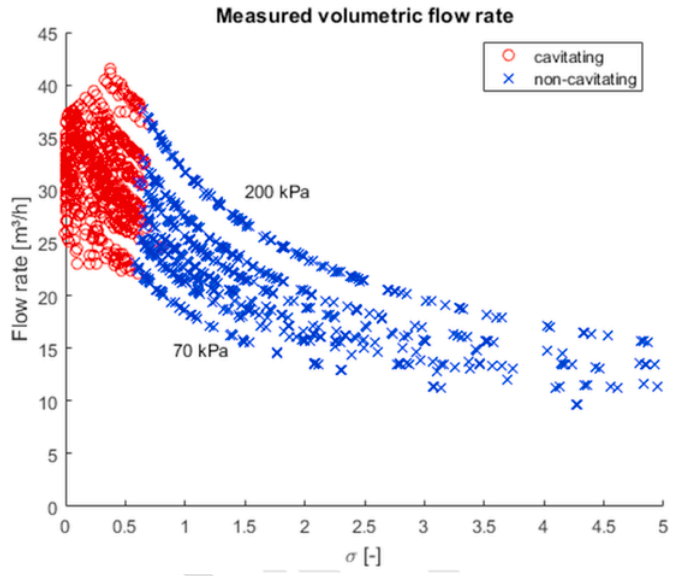

Fig. 9. Measured volumetric flow rate as a function of the cavitation number. Blue crosses correspond to non-cavitating regime and red circles correspond to cavitating regimes. (For interpretation of the references to colour in this figure legend, the reader is referred to the Web version of this article.)

Our results show a near stochastic dispersion over the region with lower cavitation numbers when cavitation appears and an hyperbolic trend in non-cavitating flows with a strong influence of the pressure level as stated by Abdulaziz [7]. Nevertheless, the blockage of the test section with constant mass flow rates below critical cavitation number revealed by Abdulaziz are not reproduced by our results. Here it must be noted that Abdulaziz kept constant the Venturi inlet pressure while in our experiments we kept constant the reference pressure.

4.4. Discharge coefficient behaviour

The Venturi's discharge coefficient, C, has been calculated for all tested operating points based on the recommendations given by the standard ISO 5167 [3] and it has been plotted as a function of Reynolds in Fig. 10. This standard indicates that C is valid for Reynolds numbers above 2×10^6 and for Venturis with diameter ratios β between 0.30 and 0.75. The standard also provides figures for Reynolds number from 4×10^4 but with worse uncertainty.

The plot shows two different trends depending on the flow regime. For non-cavitating flows, C increases slightly with Reynolds and presents significantly greater values than those reported by Reader-Harris et al. [21] and by the standard [3]. On the contrary, C presents lower values in cavitating regimes and shows some dependency with the cavity length as it can be confirmed in Fig. 11 where the longest cavities present smaller discharge coefficients.

It must also be noted that our results are in agreement with the statement found in Ref. [3] about the observed slightly decrease of C for regimes of operation under Reynolds values of 2×10^5.

When the discharge coefficient is plotted as a function of the Venturi's pressure ratio or the cavitation number as shown in Fig. 12 and Fig. 13, respectively, all the points collapse to a single trend along the entire range of operating conditions. As can be seen in both graphs, a clear change of behaviour is identified between non-cavitating and cavitating flow conditions.

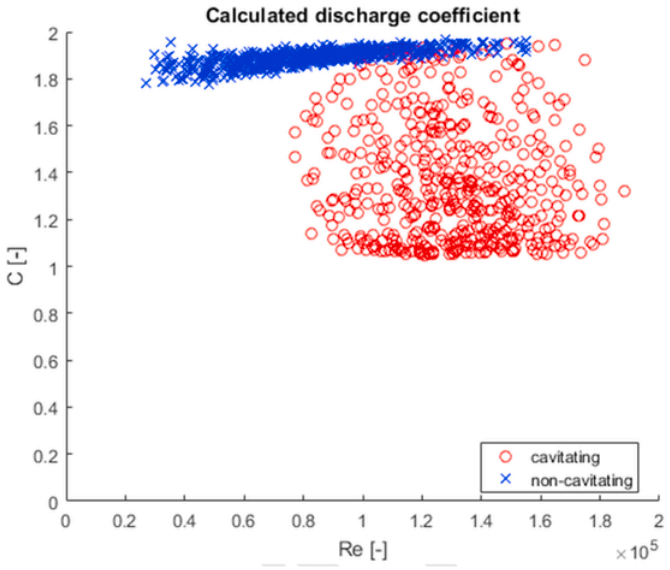

Fig. 10. Calculated discharge coefficient as a function of Reynolds number for any operating condition. Blue crosses correspond to non-cavitating regime and red circles correspond to cavitating regimes. (For interpretation of the references to colour in this figure legend, the reader is referred to the Web version of this article.)

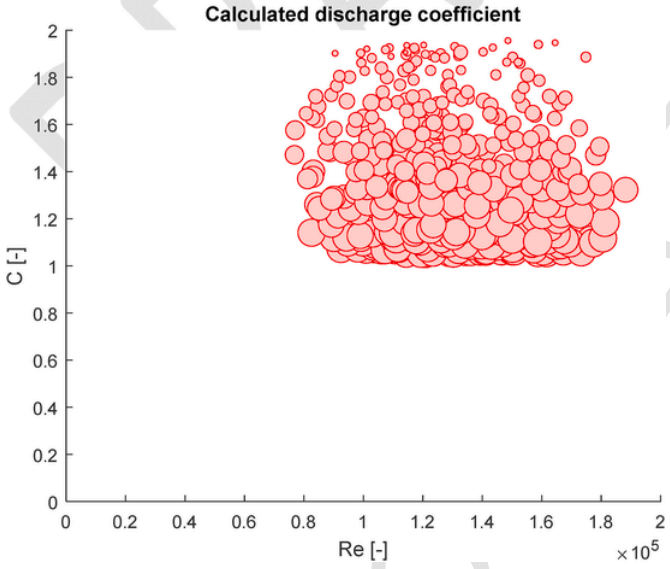

Fig. 11. Calculated discharge coefficient as a function of Reynolds number for cavitating flows. The size of the markers represents the length of the observed cavity.

Analogous results can be found using the pressure loss coefficient, ζ, as shown in Figs. 14 and 15. The value of ζ keeps constant in non-cavitating flows but it increases linearly as the pressure ratio drops (Fig. 14) and the cavitation number decreases (Fig. 15). Rudolf et al. [8] developed a useful tool based on the behaviour of the pressure loss coefficient that permitted to identify different cavitating regimes in axisymmetric Herschel-Venturi tubes while Brinkhorst et al. [22] employed the experimental results to validate cavitation models with numerical simulations and to study the effects of different geometrical parameters [10]. The numerical results showed a similar behaviour despite the narrow range of simulated operational points and a sensible difference between the experimental and numerical results. It must be noted that the present experiments cover a larger range of operational points than those covered by these previous studies.

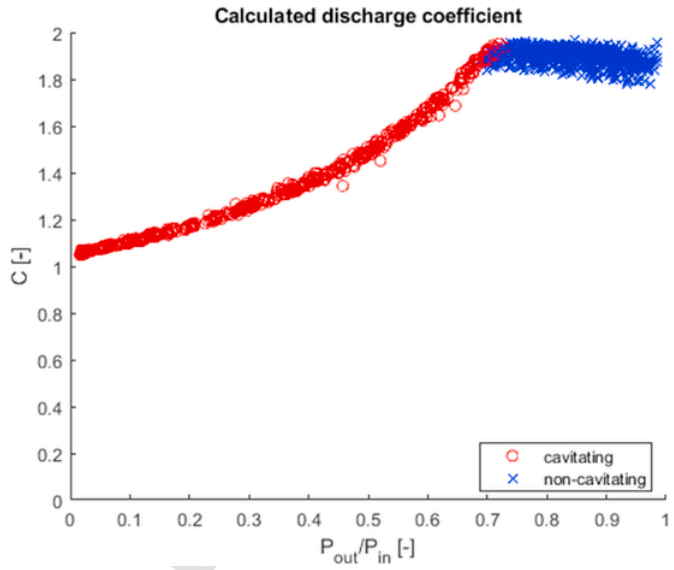

Fig. 12. Discharge coefficient as a function of pressure ratio. Blue crosses correspond to non-cavitating regime and red circles correspond to cavitating regimes. (For interpretation of the references to colour in this figure legend, the reader is referred to the Web version of this article.)

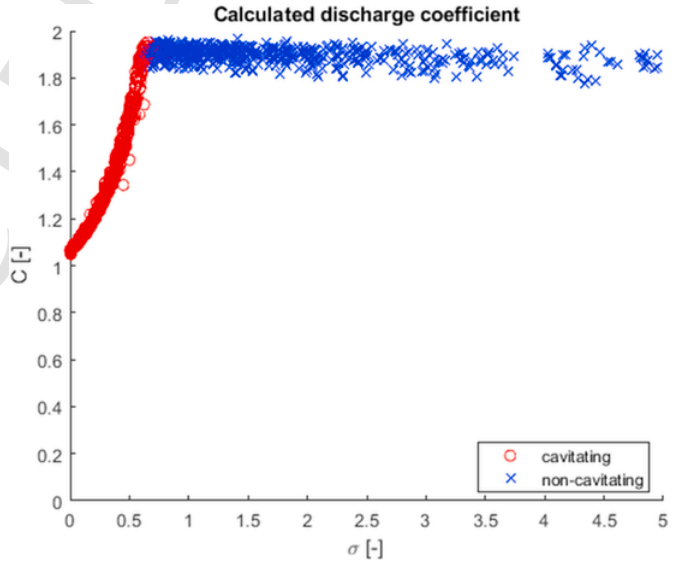

Fig. 13. Discharge coefficient as a function of cavitation number. Blue crosses correspond to non-cavitating regime and red circles correspond to cavitating regimes. (For interpretation of the references to colour in this figure legend, the reader is referred to the Web version of this article.)

Both the discharge and the pressure loss coefficients present excellent behaviours in non-cavitating regimes with constant values and narrow uncertainties. That is the reason why both, and specially the discharge coefficient, are used in flow metering with pressure differential devices. However, the current results and former ones presented by other authors like Rudolf [8] or Reader-Harris et al. [21] clearly show that both coefficients no longer remain constant when cavitation takes place. More specifically, the discharge coefficient drops and the pressure loss coefficient rises.

5. Flow rate coefficient for cavitating flows

The behaviour of the Venturi's inlet pressure as a function of measured volumetric flow rate is shown in Fig. 16. In non-cavitating

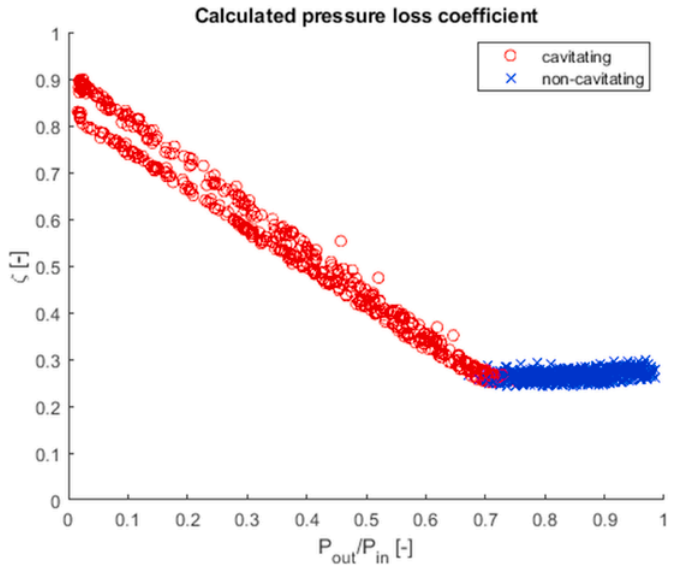

Fig. 14. Pressure loss coefficient as a function of outlet's and inlet's pressure ratio. Blue crosses correspond to non-cavitating regime and red circles correspond to cavitating regimes. (For interpretation of the references to colour in this figure legend, the reader is referred to the Web version of this article.)

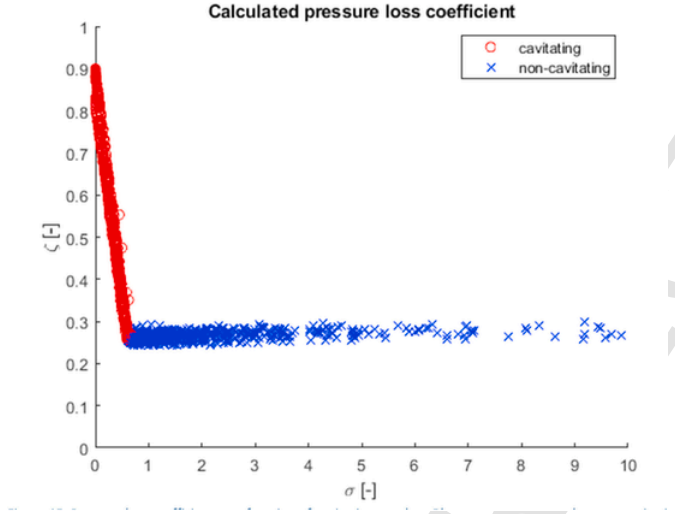

Fig. 15. Pressure loss coefficient as a function of cavitation number. Blue crosses correspond to non-cavitating regime and red circles correspond to cavitating regimes. (For interpretation of the references to colour in this figure legend, the reader is referred to the Web version of this article.)

regime, P_{in} depends on P_{ref} and its value increases slightly as the Reynolds number increases. For example, a rise of 0.3 kPa per m³/h is found for P_{ref} 200 kPa. This behaviour changes when cavitation develops inside the Venturi and all the measurements collapse into a single trend independently of P_{ref}. In these conditions, the rate at which P_{in} increases with flow rate is up to 15 times greater than that exhibited in non-cavitating regime. Hence, this behaviour confirms that the cavitating flow inside the Venturi is choked and the only way to increase the flow rate is increasing P_{in}, which is an analogous behaviour as that observed in compressible gas nozzles [21] where for any given inlet's condition the highest flow rates are only reached when the flow is chocked.

It is well known that reductions in downstream pressure do not lead to higher flow rates in choked compressible gas nozzles. Instead, only an upstream pressure increment can rise the nozzle's flow rate as equation (7) indicates:

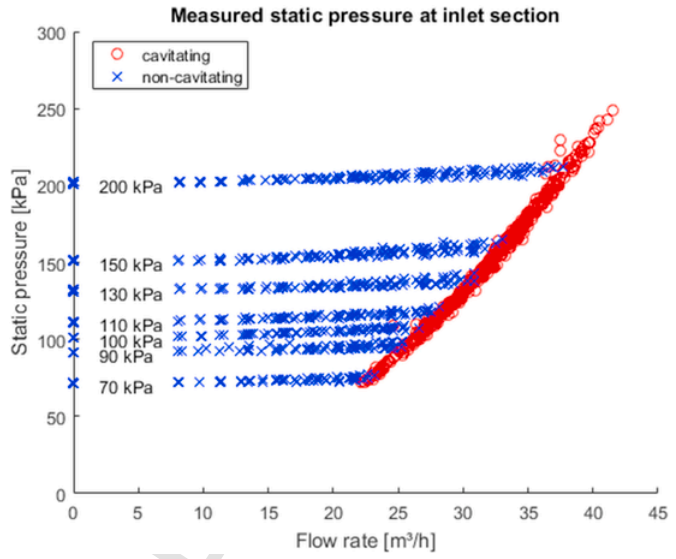

Fig. 16. Measured Venturi's inlet pressure as a function of measured volumetric flow rate. Blue crosses correspond to non-cavitating regime and red circles correspond to cavitating regimes. (For interpretation of the references to colour in this figure legend, the reader is referred to the Web version of this article.)

$$Q = \sqrt{\frac{P_{in}}{\rho(T)}} A_t \sqrt{\gamma \left(\frac{2}{\gamma+1}\right)^{\frac{\gamma+1}{\gamma-1}}} \tag{7}$$

where γ is the heat capacity ratio of the gas.

Equation (7) represents the theoretical volumetric flow rate in a converging-diverging tube with a perfect gas flowing under choked conditions. The third term of the product is a dimensionless constant that scales the result. Thus, the volumetric flow rate of a compressible gas flowing in a chocked Venturi is proportional to inlet conditions and throat area as presented in the following expression:

$$Q \propto \sqrt{\frac{P_{in}}{\rho(T)}} A_t \tag{8}$$

On the basis of the observed results and the analogy with the behaviour of chocked compressible gas nozzles, a new flow rate coefficient is proposed for cavitating Venturis which results from the adimensionalization of the volumetric flow rate with the inlet pressure, density and throat area:

$$\Theta = \frac{Q}{A_t \sqrt{\frac{P_{in}}{\rho(T)}}} \tag{9}$$

The dependency of Θ with the temperature is revealed by combining equation (6) with equation (9):

$$\Theta = \frac{\mu(T)}{\sqrt{P_{in}\rho(T)}} \left(\frac{A_t}{A_{in}}\varphi_{in}\right)^{-1} Re \tag{10}$$

The expanded form of equation (9) suggests that Θ is proportional to the Reynolds number. However, that proportionally depends not only on the water temperature but also on the Venturi's inlet static pressure.

This new flow rate coefficient has been plotted as a function of Reynolds number in Fig. 17 and the resulting plot resembles the behaviour already observed in Fig. 6 where the volumetric flow rate has been plotted as a function of Re. Fig. 17 shows the expected proportionality of Θ with Re and an upper value around 1.48 which cannot be

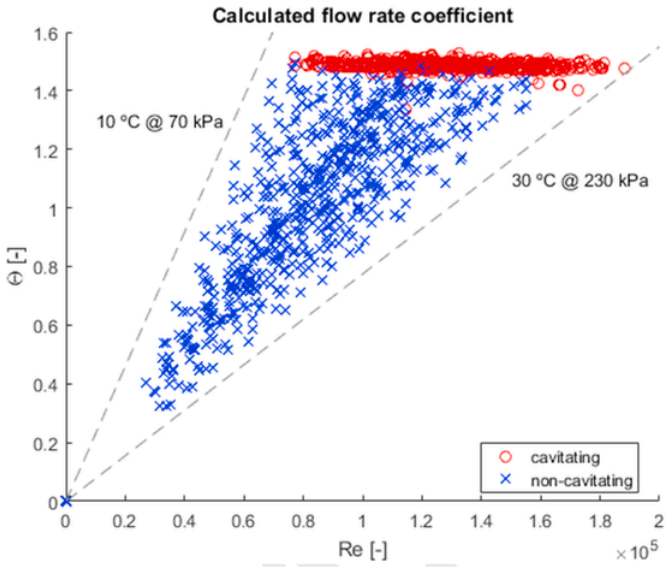

Fig. 17. New flow rate coefficient as a function of Reynolds number. Dashed lines represent the limits of the experimental temperature range. Blue crosses correspond to non-cavitating regime and orange circles correspond to cavitating regimes. (For interpretation of the references to colour in this figure legend, the reader is referred to the Web version of this article.)

exceeded. The operating points located on this upper limit correspond to measurements taken with cavitation regimes only.

On the other hand, Fig. 18 just presents those values of Θ at P_{ref} 70 and 200 kPa. In non-cavitating regime, Θ exhibits a linear dependency with Re until cavitation appears inside of the Venturi. From this value and for higher Re, Θ is constant.

The representation of Θ in front of the pressure ratio (see Fig. 19) shows a completely different behaviour compared to the one observed with the discharge and pressure loss coefficients. Θ remains constant in any cavitating regime and only varies at non-cavitating regimes. Even so, Θ is independent of P_{ref} as the discharge and loss coefficients. For operating conditions with pressure ratios above 0.7, Θ decreases progressively from 1.49 to 0 as the pressure ratio increases. All these points correspond to non-cavitation conditions. But for pressure ratios

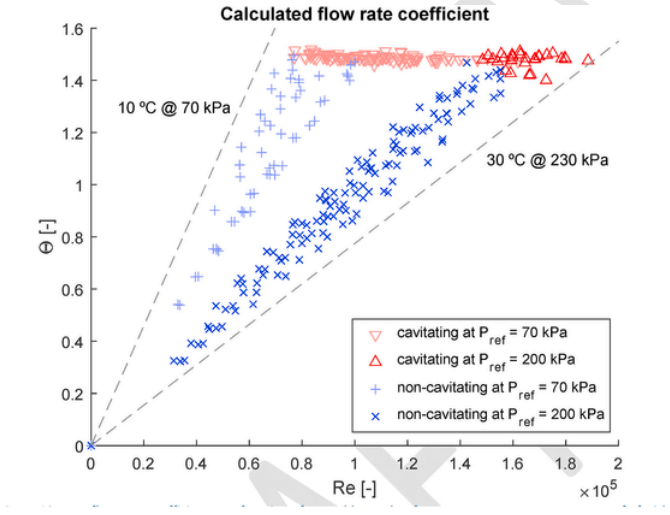

Fig. 18. New flow rate coefficient as a function of Reynolds number for measurements at constant P_ref of 70 kPa (soft colored blue crosses and red triangles) and 200 kPa (saturated blue crosses and red triangles). (For interpretation of the references to colour in this figure legend, the reader is referred to the Web version of this article.)

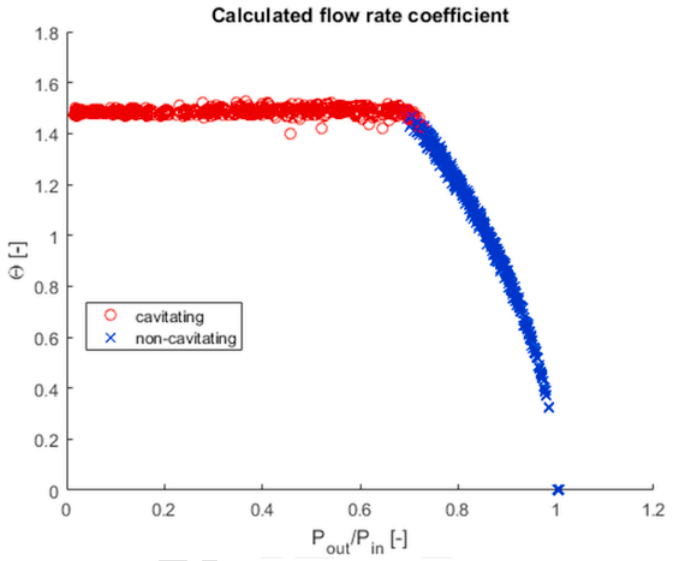

Fig. 19. New flow rate coefficient as a function of pressure ratio. Blue crosses correspond to non-cavitating regime and red circles correspond to cavitating regimes. (For interpretation of the references to colour in this figure legend, the reader is referred to the Web version of this article.)

below 0.67, Θ keeps constant at 1.49 for any type of cavitation regime takes place within the Venturi.

It can be stated that Θ exhibits an excellent behaviour in cavitating regimes with a constant value independently of the pressure ratio. Therefore, if a converging-diverging geometry has been previously characterized, the flow rate can be predicted using equation (9) and measuring the Venturi's inlet pressure. It must be noted that the existing discharge and pressure loss coefficients can predict flow rates only for converging-diverging geometries in non-cavitating regimes.

As summarized in Table 1, the equations to be used for measuring volumetric flow rates of water in Venturis as a function of the presence or absence of cavitation within the flow. The discharge coefficient should be used in non-cavitating regimes for pressure ratios above 0.71. The new flow coefficient should be used in regimes with pressure ratios below 0.67 at cavitating regimes. Authors also recommend to avoid the transition between both regimes in the range from 0.67 to 0.071 since the flow rate prediction might lack accuracy. For both coefficients, a series of calibration tests with a given converging-diverging geometry must be preliminary performed in order to determine their values with low uncertainty.

6. Conclusions

The flow performance of the present asymmetric Venturi under non-cavitation and cavitation flow conditions is consistent with previous experimental and numerical studies even though slight geometrical differences exist such as the cross section shape, the converging/diverging angles and the hydraulic diameter ratio.

Table 1
Proposed pressure ratio ranges and equations to calculate the volumetric flow rate in a Venturi in the whole operating range.

Non-cavitating regime	Transition regime	Cavitating regimes
$1>\frac{P_{out}}{P_{in}}>0.71$	$0.71>\frac{P_{out}}{P_{in}}>0.67$	$0.67>\frac{P_{out}}{P_{in}}>0.00$
Discharge coefficient $Q = A_t\sqrt{\frac{2}{\rho}\Delta P}\, C\frac{1}{\sqrt{1-\beta^4}}$	*Region to avoid* –	*Flow coefficient* $Q = A_t\sqrt{\frac{P_{in}}{\rho(T,\,P)}}\Theta$

The tests carried out show that a Venturi presents a different behaviour depending on the presence of cavitation or not. The cavitation inception in the throat takes place at a pressure ratio between the Venturi's inlet and outlet sections between 0.67 and 0.71, which is close to the results found by Abdulaziz [7] who also reported a value in the range from 0.7 to 0.72.

The volumetric flow rate appears to be dependent on Venturi's inlet pressure at cavitating regimes. The Venturi's inlet pressure must be increased in order to rise the flow rate as it also required for compressible gas nozzles with choked flows.

A new flow rate coefficient has been proposed that permits to use a Venturi like geometry as a flow meter device under cavitation conditions based on its inlet pressure. This flow rate coefficient shows a constant value for any cavitation size and morphology but changes for non-cavitating regimes. Thus, a single converging-diverging geometry could become a more versatile flow meter if it is characterized not only by its discharge coefficient (or pressure loss coefficient) but also by its flow rate coefficient. The first coefficient is suitable for measurements above a pressure ratio of 0.71 and second one is suitable for regimes below 0.67.

New experiments should be performed with different converging-diverging geometries in order to validate the reliability of the new flow rate coefficient. Moreover, the influence of the water temperature in the flow rate coefficient should also be studied in a series of tests where the water temperature in the system is kept constant.

Credit author statement

David Bermejo: Conceptualization, Methodology, Validation, Formal analysis, Investigation, Data Curation, Writing - Original Draft, Visualization, **Xavier Escaler**: Conceptualization, Writing - Reviewing & Editing, Supervision, **Rafael Ruíz-Mansilla**: Supervision, Funding acquisition.

Uncited reference

Declaration of competing interest

The authors declare that they have no known competing financial interests or personal relationships that could have appeared to influence the work reported in this paper.

Acknowledgement

This study was financed by the regional government of Catalonia, through its program of Industrial Doctorates, and the environmental engineering company Condorchem Envitech, S.L. The authors would like to thank Sergio Tuset (CEO of Condorchem Envitech, S.L.) for sponsoring personally the associated research project.

References

[1] C.E. Brennen, Cavitation and Bubble Dynamics, Oxford University Press, Oxford, 1995.
[2] Technical Committee ISO/TC 30/SC 2, ISO 9300:2005 - Measurement of Gas Flow by Means of Critical Flow Venturi Nozzles, International Organization for Standardization, 2005.
[3] Technical Committee ISO/TC 30/SC 2, ISO 5167-4:2003 - Measurement of Fluid Flow by Means of Pressure Differential Devices Inserted in Circular Cross-Section Conduits Running Full - Part 4: Venturi Tubes, International Organization for Standardization, 2003.
[4] L.N. Randall, Rocket applications of the cavitating Venturi, J. Am. Rocket Soc. 22 (1) (1952) 28–38.
[5] A. Ulas, Passive flow control in liquid-propellant rocket engines with cavitating venturi, Flow Meas. Instrum. 17 (2) (2006) 93–97 April.
[6] M. Zamoum, M. Kessal, Analysis of cavitating flow through a venturi, Sci. Res. Essays 10 (11) (2015) 367–375 15 June.
[7] A.M. Abdulaziz, Performance and image analysis of a cavitating process in a small type Venturi, Exp. Therm. Fluid Sci. 53 (2014) 40–48.
[8] P. Rudolf, M. Hudec, M. Gríger, D. Stefan, Characterization of the cavitating flow in converging-diverging nozzle based on experimental investigations, EPJ Web Conf. 67 (2014) 25 Marzo 02101.
[9] B. Charrière, J. Decaix, E. Goncalvès, A comparative study of cavitation models in a Venturi flow, Eur. J. Mech. B Fluid 49 (2015) 287–297.
[10] S. Brinkhorst, E. von Lavante, G. Wendt, Numerical investigation of cavitating Herschel Venturi-Tubes applied to liquid flow metering, Flow Meas. Instrum. 43 (2015) 23–33.
[11] M. Dular, I. Khlifa, S. Fuzier, M. Adama Maiga, O. Coutier-Delgosha, Scale effect on unsteady cloud cavitation, Exp. Fluid 53 (5) (2012) 1233–1250.
[12] J. Decaix, E. Goncalvès, Investigation of three-dimensional effects on a cavitating Venturi flow, Int. J. Heat Fluid Flow 44 (2013) 576–595.
[13] J.R. Cooper, R.B. Dooley, "Revised Release on the IAPWS Industrial Formulation 1997 for the Thermodynamic Properties of Water and Steam," International Association for Properties of Water and Steam, Lucerne, Switzerland, 2007.
[14] D. Bermejo Plana, F.X. Escaler Puigoriol, R. Ruíz Mansilla, Mapping Venturi cavitation in a new closed loop facility devoted to study thermodynamic effects, Proceedings of the 3rd International Symposium of Cavitation and Multiphase Flow, 2019 ISCM2019.
[15] Technical Committee ISO/TC 115/SC 2, ISO 9906:2012 - Rotodynamic Pumps -- Hydraulic Performance Acceptance Tests -- Grades 1, 2 and 3, International Organization for Standardization, 2012.
[16] H. Ghassemi, H.F. Fasih, Application of small size cavitating venturi as flow controller and flow meter, Flow Meas. Instrum. 22 (2011) 406–412.
[17] Joint Committee for Guides in Metrology, Working Group 1, JCGM 100:2008 - Evaluation of Measurement Data — Guide to the Expression of Uncertainty in Measurement, Bureau International des Poids et Mesures, 2008.
[18] J.R. Cooper, R.B. Dooley, Release on the IAPWS Formulation 2008 for the Viscosity of Ordinary Water Substance, " International Association for Properties of Water and Steam, Berlin, Germany, 2008.
[19] L.F. Moody, Friction factors for pipe flow, Trans. ASME 66 (8) (1944) 671–684.
[20] S. Brinkhorst, E. von Lavante, D. Güler, G. Wendt, "Experimental Investigation of Cavitating Herschel Venturi-Tube Configuration," 17th International Flow Measurement Conference, FLOMEKO, Setiembre, 2016.
[21] M.J. Reader-Harris, W.C. Brunton, J.J. Gibson, D. Hodges, I.G. Nicholson, Discharge coefficients of Venturi tubes with standard and non-standard convergent angles, Flow Meas. Instrum. 12 (2001) 135–145.
[22] S. Brinkhorst, E. von Lavante, G. Wendt, "Numerical Investigation of Effects of Geometry on Cavitation in Herschel Venturi-Tubes Applied to Liquid Flow Metering," International Symposium on Fluid Flow Measurement, 2015 ISFFM2015.
[23] P. Balachandran, Fundamentals of Compressible Fluid Dynamics, PHI Learning Private Limited, New Delhi, 2006.